


Predicting yielding in attractive colloidal gelsDeepak Mangal , Mohammad Nabizadeh, and Safa Jamali**Department of Mechanical and Industrial Engineering, Northeastern University, Boston, Massachusetts 02115, USA*

(Received 28 March 2023; accepted 6 December 2023; published 5 January 2024)

One of the defining characteristics of soft glassy materials is their ability to exhibit a yield stress, which can result in an overall elasto-visco-plastic mechanics. To design soft materials with specific properties, it is essential to gain a comprehensive understanding of the topological and structural failure points that occur during yielding. However, predicting these failure points, which lead to yielding, is challenging due to the dynamic nature of structure development and its cooccurrence with other complicated processes, such as local rearrangements and anisotropy. In this study, we employ a series of tools from network science to investigate colloidal gels as a model for soft glassy materials during yielding. Our findings reveal that edge betweenness centrality can be utilized as a universal predictor for yielding across various state variables, including the volume fraction of solids, the strength, and the range of attraction between colloids.

DOI: [10.1103/PhysRevE.109.014602](https://doi.org/10.1103/PhysRevE.109.014602)**I. INTRODUCTION**

Amorphous soft glassy materials are prevalent in both natural and industrial settings. These disordered systems typically show solidlike behavior until a critical point, known as the yield stress, is reached under applied deformation or load. Beyond this stress threshold, the material undergoes irreversible microstructural events and starts to flow [1]. Considerable research has been conducted on attractive colloidal gels with low and intermediate solid volume fractions as a model for soft glassy materials [2–8]. During a yielding event under deformation, these space-spanning particle networks undergo various microstructure changes, including local rearrangement, structural anisotropy, and network rupture [9–19]. The network may also experience stress-strain inhomogeneities [11,15]. Furthermore, the microstructure undergoes simultaneous reformation resulting in complex rate- and time-dependent rheological behavior [20]. Despite these complexities, a micromechanistic understanding of yielding and the onset of flow has emerged. The localization of stress and strain in elastically deformed particle-particle bonds, followed by their rupture, causes the localized and irreversible plastic rearrangements. These rearrangements facilitate the relaxation of the particle chain or network [6,15,21,22]. While we generally understand the sequence of local events leading to overall yielding, we still have limited knowledge about the specific characteristics of these local environments and the early stages of yielding. As a result, the structural precursors to yielding remain largely unknown. Therefore, it is crucial to comprehend the bonds and particles that are susceptible to these microscale rupture events and ultimately are responsible for gel yielding. This understanding will facilitate the targeted design of soft glassy materials with appropriate yield stresses.

The rate-dependent rheology of colloidal gels in a quasi-steady state can be characterized by considering the lifetime of colloidal bonds [23]. However, during yielding, the lifespan of a bond depends on whether the colloids sharing the bond reside within the bulk of gel structure or on its surface, and is thus not a reliable indicator of whether a bond would break under applied deformation. In our most recent investigation of weakly attractive colloidal gels, the bond rupture events were found to have a significant correlation with the orientation and network centrality of the bonds [24]. In this study, we explore various state variables, including attraction strengths/range and solid concentration, to develop a comprehensive understanding of structural yielding predictions in soft glassy materials.

II. METHODS

In this study, a system of monodisperse colloid particles with radii $a = 1$ in a cubic box with periodic boundary conditions is simulated using the core-modified dissipative particle dynamics (CM-DPD) method [16,24–26]. To conduct studies at $0.2 \leq \phi \leq 0.4$ concentrations, a constant number of colloid particles ($n_C = 10\,000$) are used with changing amounts of solvent particles. The attraction between colloid particles is modeled using a Morse potential $U_{\text{Morse}} = U_0(2 \exp^{-\kappa h_{ij}} - \exp^{-2\kappa h_{ij}})$, where U_0 and κ^{-1} are the depth and range of attraction well. The range of attractive strengths of $6 \leq U_0/k_B T \leq 20$, representing weak to strong interactions, with $7 \leq \kappa a \leq 30$ (or range $0.1a$ to $0.5a$), representing short- to long-range attractions are systematically varied at a dimensionless kinetic temperature of $k_B T = 0.1$. The simulations consist of two steps. First, colloid gel structures are generated by running simulations under quiescent conditions for approximately $\sim 300\tau_D$, where $\tau_D = \pi \eta a^3 / k_B T$ is the diffusion time of a bare colloidal particle, and η is solvent viscosity. During this step, we ensure that a quasi-steady structure is reached without significant alterations to

*s.jamali@northeastern.edu

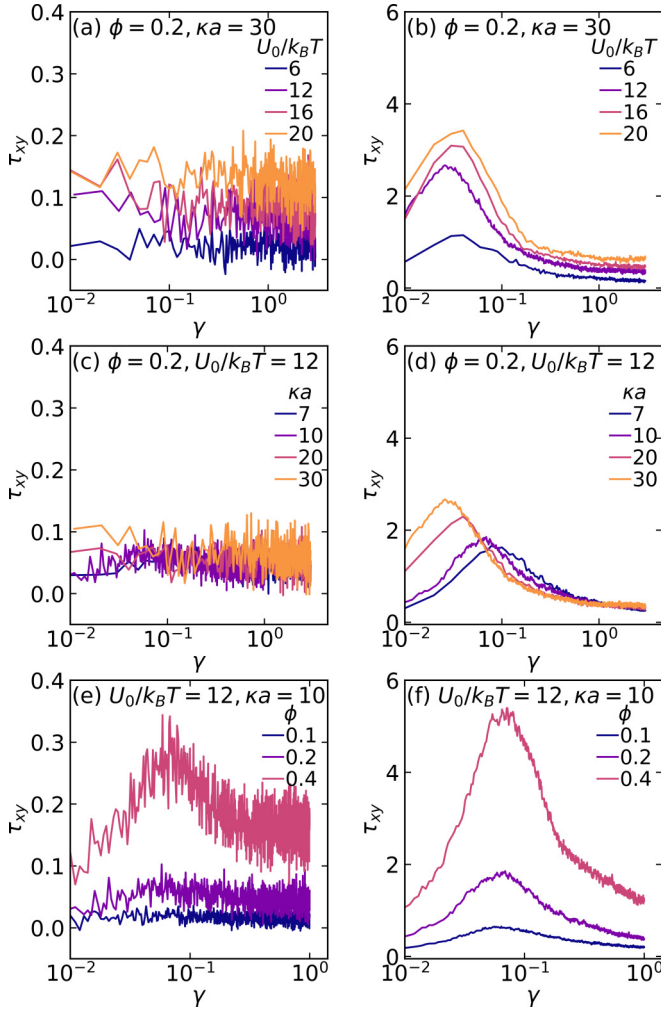


FIG. 1. Stress-strain response of colloidal gel at Mn values of (a), (c), (e) 0.2 and (b), (d), (f) 8.6. Data for $U_0/k_B T = 6$ at $\kappa a = 30$ and $\phi = 0.2$ are taken from Ref. [24].

the microstructure. In the second step, the gels are subjected to a simple shear flow with different deformation rates, $\dot{\gamma}$, using a Lees-Edward boundary condition [27]. Throughout the study, the deformation rate is quantified as the ratio of convective shear force to the attraction force, expressed by the dimensionless Mason number $Mn = 6\pi\eta\dot{\gamma}a^3/U_0$ [23,28,29]. All simulations are performed using HOOMD blue [30], an open-source molecular dynamics simulation toolkit.

III. RESULTS AND DISCUSSION

The stress response for two different Mason numbers as a function of applied strain is shown in Fig. 1. Regardless of the applied Mn, shear stress generally shows an overshoot followed by a rather long transient decay to a quasisteady state value. The stress overshoot serves as a hallmark of yielding behavior and the departure from the linear viscoelastic response, while the long-time transient stress response indicates the thixotropic restructuring of the system [15,21,31]. Note that at low Mason numbers, Brownian forces can play a significant role and screen some of the stress overshoot as well [Figs. 1(a) and 1(c)]. This behavior aligns with findings

from previous experiment and simulation studies, where stress overshoot is absent for very low shear rate, and rises as shear rate increases [17,18,32]. Similar behavior has also been observed in colloidal glass [33]. In the case of variable strength with fixed $\kappa a = 30$ and $\phi = 0.2$, this stress overshoot increases with strength, whereas the critical strain at the maximum stress is unchanged [Fig. 1(b)]. The overshoot also increases with κa with fixed strength $U_0/k_B T = 12$ and $\phi = 0.2$, whereas the critical strain at the maximum stress shifts to a lower strain value [Fig. 1(d)]. Finally, while retaining a given strength and range, we examine the stress response for various particle volume fractions, ϕ . Since there are more particle interactions as ϕ grows, stress overshoot is seen to increase dramatically, while the critical strain at maximum remains essentially the same [Figs. 1(e) and 1(f)]. As a whole, this demonstrates that the critical strain is determined by the range of attraction, whereas the number of contacts and strength of the attraction force determines the stress overshoot.

In their seminal work, Colombo and Del Gado proposed the predominance of the bond rupture rate over the formation rate serves as a criterion for the dynamic yield of attractive gels [15]. We track the kinetics of bond formation and breakup in the gel by having access to all colloidal bonds during deformation. The interparticle bonds are dynamically formed and broken throughout the simulation due to the combined effects of thermal fluctuations, the natural affinity of particles to bond, and the shearing forces trying to rupture them [15,34]. Figure 2 shows the average coordination number relative to the quiescent value as a function of applied strain for the same two applied Mason numbers. The total number of bonds initially remains constant even under stronger shearing forces ($Mn = 8.6$), but with large strains ($\gamma > 0.1$) they naturally start to monotonically decline, indicating the fluidization of the structure. On the other hand, nonmonotonic changes are observed at lower applied deformation rate ($Mn = 0.2$), which may indicate early compaction (for longer ranges of attraction or higher solid fractions) or initial breakage followed by secondary structure formation (for short range attractions). While the critical strain at which the total number of bonds begins to decay is somewhat independent of the attraction strength and marginally reliant on the volume fraction of solids, it clearly trends toward greater strains as the attraction range increases [Figs. 2(c) and 2(d)]. When comparing the average coordination numbers in Figs. 2(a), 2(c), and 2(e) vs 2(b), 2(d), and 2(f), it should be noted that at lower applied Mason numbers, the coordination number of particles within the particle clusters can be large, resulting in an overall number of contacts that remains close to the gel state despite significant structural and mechanical differences between these “flowing” aggregated structures and “unyielded” gel structures. Additionally, even though the total number of bonds does not drop at the start of deformation ($\gamma \lesssim 0.1$), this does not imply that no bonds have been broken. The number of newly formed and ruptured bonds per particle for two different Mason numbers as a function of applied strain is shown in Fig. 3. For small $Mn = 0.2$, the number of newly formed and ruptured bonds nearly balances each other, therefore we see negligible changes in the evolution of average coordination numbers, as illustrated in Fig. 1. At big $Mn = 8.6$, however, the number of ruptured bonds is high,

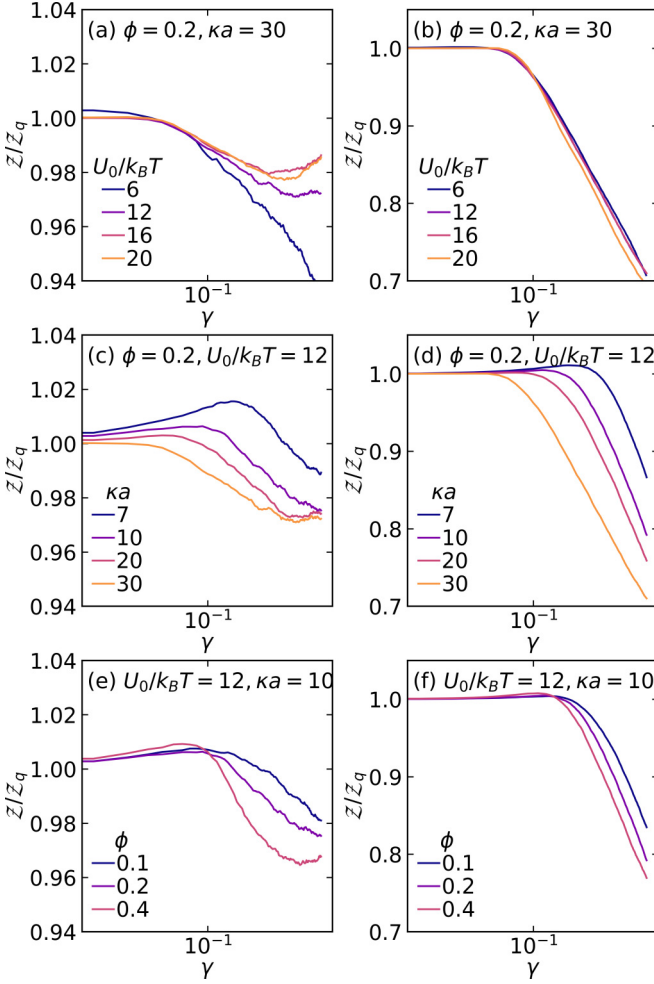


FIG. 2. Evolution in the ensemble-averaged coordination number relative to the quiescent value as a function of strain γ at two different applied Mason numbers of (a), (c), (e) $Mn = 0.2$ and (b), (d), (f) $Mn = 8.6$. Role of different state variables on the overall bond loss rate is explored: (a), (b) Attraction strength is changed from weak to strong, keeping the interaction range and volume fraction constant; (c), (d) Attraction range is changed from short to long range, keeping their strength and volume fraction constant; and (e), (f) Colloid volume fraction is varied at constant pair particle interaction. Data for $U_0/k_B T = 6$ at $\kappa a = 30$ and $\phi = 0.2$ are taken from Ref. [24].

and considerably fewer bonds are formed because the bond dynamics is now primarily controlled by the strong shear forces.

Yielding of soft glassy materials, in general, can be a complex concept that may lack a universally accepted description [1]. However, in this study, we confidently conclude that the gel has yielded at $\gamma = 1$ based on visual inspection of the flowing system, velocity profiles, and rheological responses during gel deformation. Therefore, the bonds that break within the initial unit of applied strain are considered responsible for the yielding of the gel structure. In the first step, we identify and mark these bonds throughout the structure of the quiescent gel prior to deformation. Our objective is to determine the most characteristic feature of these broken bonds. Our recent findings indicate that the coordination number of the

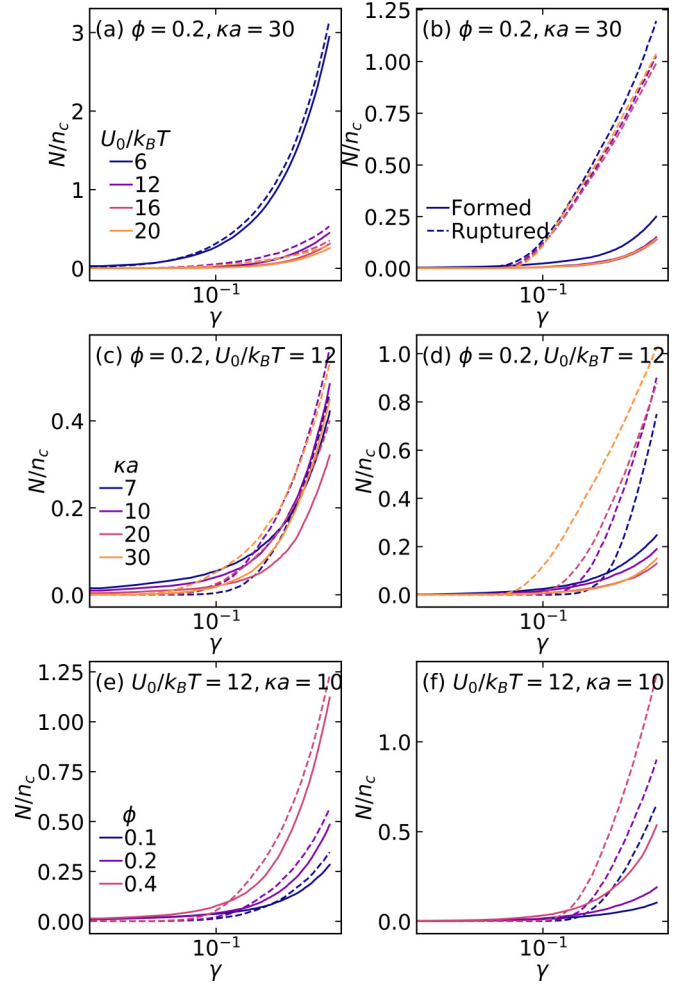


FIG. 3. Number of newly formed and ruptured bonds per particle at Mn values of (a), (c), (e) 0.2 and (b), (d), (f) 8.6. Data for $U_0/k_B T = 6$ at $\kappa a = 30$ and $\phi = 0.2$ are taken from Ref. [24].

bond-sharing particles or their lifetime under gelation does not exhibit any correlation with the occurrence of broken bonds during initial yielding of the structure [24]. On the other hand, it is well established that bonds within the gel structure that accumulate strains/stresses lead to localized microyielding events. However, localization of the stress/strain does not necessarily align with the states of self-stress or particle-level measures of the system. Instead, a global network-level measure must be considered to pinpoint the bonds with the highest degrees of strain localization. This is because the rupture event itself, and the following relaxation of the bonds following a rupture, propagates through the particle network. To establish a correlation between bond characteristics and the yielding behavior, it is imperative to employ a network-level measure. In this study, we represent the gel structure as a single connected component encompassing all particles. Figures 4(a) and 4(b) provide a schematic representation of a gel structure depicted as a network of nodes and edges. In any interconnected network, edge betweenness centrality (EBC), denoted as B_{ij} , precisely defines the characteristic of each edge or bond as a numerical indicator of its importance to the entire network. EBC inherently captures both global and

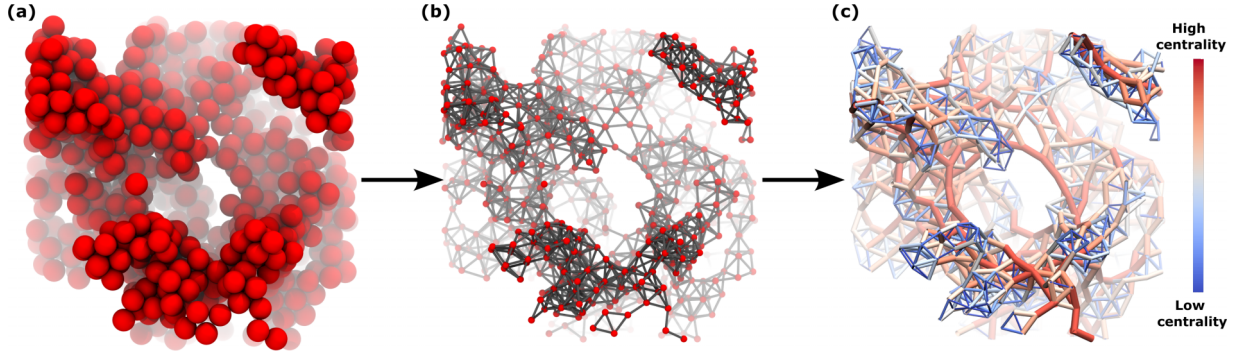


FIG. 4. (a) A typical snapshot of colloidal gel structure, (b) representation of the same structure as a network of nodes and edges, and (c) visualizing the EBC values for a typical colloidal network.

local features of the network. The calculation of EBC for a bond in any given network is based on the percentage of all shortest paths between network pairs that traverse the bond. The EBC value of a bond e in the network is computed as

$$B_{ij} = \sum_{a \neq b} \sigma(a, b|e) / \sigma(a, b), \quad (1)$$

where $\sigma(a, b)$ is the total number of shortest pathways connecting every pair of a and b nodes in the system, and $\sigma(a, b|e)$ is the number of shortest paths that include bond e in their sequence. In Fig. 4(c), higher EBC values within the network are color coded with warmer colors, indicating a higher probability of these bonds appearing on the path between any given pairs of nodes within the colloidal network.

In the gel structures studied, deformation is applied to the boundaries of the calculation box, leading to a strain/stress localization at seemingly random bonds throughout the system. Our hypothesis is that bonds with a higher likelihood of being involved in the transmission of stress and strain across the structure are more likely to experience stress localization. Conversely, the removal of a bond with higher edge betweenness centrality (compared to lower EBC values) will have a significant impact on the communication between remaining pairs of nodes through their shortest paths. This can result in a loss of overall load-bearing pathways within the system.

Recent research has also demonstrated that locations with high centrality are the potential sites of failure in disordered materials [35].

Figure 5 illustrates the probability distribution of the edge betweenness centrality of the bonds in the quiescent gel structure prior to shear deformation. The distributions generally exhibit a wide power-law tail, resembling a Gamma distribution, as indicated by the dashed lines. Only a small fraction of bonds exhibit high centrality. Our recent research has demonstrated that the loss of these high centrality bonds significantly impacts the overall modulus of the gel [36]. For a fixed attraction range and constant particle concentration, the distribution widens minimally by changing the attraction strength from $U_0/k_B T = 6$ to $U_0/k_B T = 30$ [Fig. 5(a)]. Similarly, the EBC distribution shows slight variations when the attraction range is changed from short to long range [Fig. 5(b)]. On the contrary, increasing the volume fraction of solids results in a nonmonotonic pattern of change in EBC, with a relatively short power-law tail. At higher concentrations, there is a relatively short power-law tail due to the significant increase in pathways between different pairs of particles within the structure, resulting in a more uniform distribution of centralities [Fig. 5(c)].

Given that the bonds broken during yielding and their initial EBC values are known, it becomes straightforward to calculate the probability function of bond rupture based

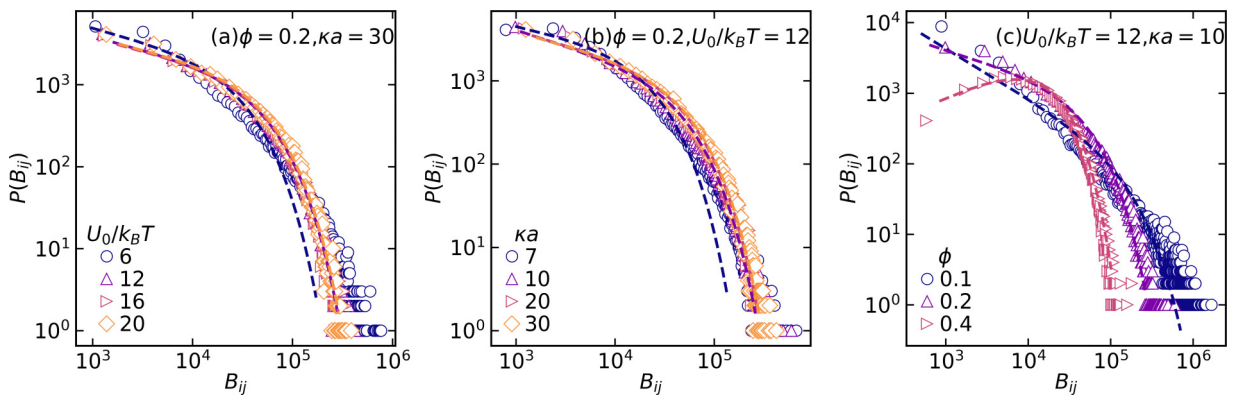


FIG. 5. Probability distributions of edge betweenness centrality of quiescently formed colloidal gels with different: (a) attraction strengths, (b) attraction ranges, and (c) volume fractions of solid. The dashed lines represent the Gamma function's fit to the distributions. Data for $U_0/k_B T = 6$ at $\kappa a = 30$ and $\phi = 0.2$ are taken from Ref. [24].

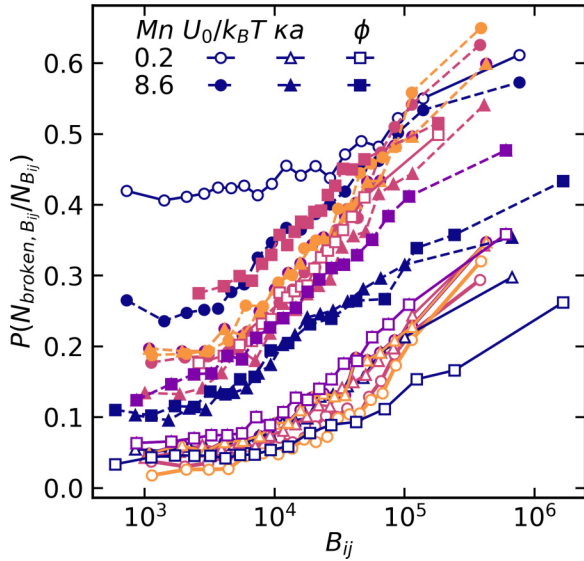


FIG. 6. Probability of bond rupture for different populations of edge betweenness centralities for colloidal gels with different attraction strengths (\circ), attraction range (Δ), and solid volume fraction (\square), under one unit of strain at the two different rates of $Mn = 0.2$ (open symbols) and 8.6 (filled symbols). Warmer hues are used to color-code data for increasing attraction strength, range, and solid volume fraction. Data for $U_0/k_B T = 6$ at $\kappa a = 30$ and $\phi = 0.2$ are taken from Ref. [24].

on EBC. Figure 6 presents the fraction of bonds that have ruptured relative to their original edge betweenness centrality for a total applied deformation of $\gamma = 1.0$. To obtain this measurement, EBC distributions are divided into 20 equal percentiles based on the power-law characteristic of the distribution, and the fraction of broken bonds is then determined for each partition. For instance, a $P(N_{\text{broken}, B_{ij}}/N_{B_{ij}}) = 0.3$ indicates that 30% of the bonds with that specific EBC value are broken during this deformation period. Regardless of the variation in state variables, the results in Fig. 6 clearly indicate that the bonds with higher centralities are more frequently broken in both applied Mason numbers. In virtually all cases studied, more than half of the bonds with high EBC values are broken within the first unit of applied strain. This finding is significant, particularly considering the fact that within this relatively small deformation window, only a very small fraction of the total bonds are broken. Even for very weak and short-range attractions, where natural bond rupture due to thermal fluctuations increases the likelihood of bond rupture overall, the general trend remains consistently unchanged. It is important to note that the threshold $\gamma = 1.0$ is not a rigid cutoff. We observed no significant change in behavior when adjusting this critical strain value used to determine the fraction of broken bonds around that point. One could, however, pose a question: if bonds with higher EBCs are more likely to localize stresses, why are not all of them ruptured

during yielding? Figure 4(c) illustrates that bonds with high EBC values are commonly found adjacent to one another, especially in strands of particles as opposed to clusters. This is because any path crossing one of these bonds inevitably crosses the other. Nevertheless, in avalanchelike yielding and fluidization of gels, similar to snap of a rubber band, when a given bond ruptures, others in its vicinity can relax and do not undergo breakage. As a result, with roughly half of the high EBC bonds broken, the entire structure can relax, and the rest of the bonds remain unbroken.

IV. CONCLUSION

In summary, this study demonstrates that edge betweenness centrality within the structure of a soft glassy system provides a robust measure of failure points during yielding events. Through systematic variation of different gelation state variables, including the strength and range of interparticle attraction, as well as the fraction of colloids, we have consistently found that high EBC bonds are the topological origins of yielding in colloidal gels. Remarkably, this unified perspective holds true regardless of the applied deformation rate, which is known to significantly influence the time-dependent structure evolution of the particle network. The network-based picture of yielding presented here is consistent with previous reports that describe yielding as a local shear localization phenomenon, also offering quantitative predictability of the specific locations of these local microyielding events.

One can engage in a meaningful discussion regarding the implications of these findings in real-world materials and experiments. To ascertain whether the EBC criterion genuinely determines bond rupture and the eventual yielding of a gel, continuous imaging of the structure during deformation is necessary, albeit more challenging. However, given the rapid advancement of experimental techniques [13,37], we remain optimistic that such experiments can and will be conducted in the future. On the other hand, since edge betweenness centrality can be utilized independently to identify failure locations within a gel structure *a priori*, and solely based on the initial topology of the particle network, it offers an approach for the targeted design of soft glassy materials. For example, one can employ different preshear or processing techniques to strengthen these high EBC modes, or deliberately design structures with desired EBC values through training of the microstructure [38–40].

ACKNOWLEDGMENTS

This work was supported by the National Science Foundation (CBET-2118962 and CBET-2104869). Computational resources were generously provided by the Massachusetts Green High-Performance Computing Center in Holyoke, MA.

[1] D. Bonn, M. M. Denn, L. Berthier, T. Divoux, and S. Manneville, *Rev. Mod. Phys.* **89**, 035005 (2017).

[2] L. Bécu, S. Manneville, and A. Colin, *Phys. Rev. Lett.* **93**, 018301 (2004).

- [3] L. Bécu, S. Manneville, and A. Colin, *Phys. Rev. Lett.* **96**, 138302 (2006).
- [4] A. Zaccone, H. Wu, and E. Del Gado, *Phys. Rev. Lett.* **103**, 208301 (2009).
- [5] E. Del Gado and W. Kob, *Phys. Rev. Lett.* **98**, 028303 (2007).
- [6] P. Jop, V. Mansard, P. Chaudhuri, L. Bocquet, and A. Colin, *Phys. Rev. Lett.* **108**, 148301 (2012).
- [7] J. Colombo, A. Widmer-Cooper, and E. Del Gado, *Phys. Rev. Lett.* **110**, 198301 (2013).
- [8] R. Benzi, T. Divoux, C. Barentin, S. Manneville, M. Sbragaglia, and F. Toschi, *Phys. Rev. Lett.* **127**, 148003 (2021).
- [9] H. Hoekstra, J. Vermant, J. Mewis, and G. Fuller, *Langmuir* **19**, 9134 (2003).
- [10] H. Hoekstra, J. Mewis, T. Narayanan, and J. Vermant, *Langmuir* **21**, 11017 (2005).
- [11] A. Mohraz and M. J. Solomon, *J. Rheol.* **49**, 657 (2005).
- [12] K. Masschaele, J. Fransaer, and J. Vermant, *J. Rheol.* **53**, 1437 (2009).
- [13] B. Rajaram and A. Mohraz, *Soft Matter* **6**, 2246 (2010).
- [14] N. Koumakis and G. Petekidis, *Soft Matter* **7**, 2456 (2011).
- [15] J. Colombo and E. Del Gado, *J. Rheol.* **58**, 1089 (2014).
- [16] A. Boromand, S. Jamali, and J. M. Maia, *Soft Matter* **13**, 458 (2017).
- [17] J. D. Park, K. H. Ahn, and N. J. Wagner, *J. Rheol.* **61**, 117 (2017).
- [18] L. C. Johnson, B. J. Landrum, and R. N. Zia, *Soft Matter* **14**, 5048 (2018).
- [19] M. Laurati, S. Egelhaaf, and G. Petekidis, *J. Rheol.* **55**, 673 (2011).
- [20] S. Jamali, G. H. McKinley, and R. C. Armstrong, *Phys. Rev. Lett.* **118**, 048003 (2017).
- [21] M. Bouzid, J. Colombo, L. V. Barbosa, and E. Del Gado, *Nat. Commun.* **8**, 15846 (2017).
- [22] R. Benzi, T. Divoux, C. Barentin, S. Manneville, M. Sbragaglia, and F. Toschi, *Phys. Rev. Lett.* **123**, 248001 (2019).
- [23] M. Nabizadeh and S. Jamali, *Nat. Commun.* **12**, 4274 (2021).
- [24] D. Mangal, M. Nabizadeh, and S. Jamali, *J. Chem. Phys.* **158**, 014903 (2023).
- [25] P. Hoogerbrugge and J. Koelman, *Europhys. Lett.* **19**, 155 (1992).
- [26] S. Jamali, A. Boromand, N. Wagner, and J. Maia, *J. Rheol.* **59**, 1377 (2015).
- [27] A. Lees and S. Edwards, *J. Phys. C* **5**, 1921 (1972).
- [28] Z. Varga, V. Grenard, S. Pecorario, N. Taberlet, V. Dolique, S. Manneville, T. Divoux, G. H. McKinley, and J. W. Swan, *Proc. Natl. Acad. Sci.* **116**, 12193 (2019).
- [29] S. Jamali, R. C. Armstrong, and G. H. McKinley, *Mater. Today Adv.* **5**, 100026 (2020).
- [30] J. A. Anderson, J. Glaser, and S. C. Glotzer, *Comput. Mater. Sci.* **173**, 109363 (2020).
- [31] S. Jamali, R. C. Armstrong, and G. H. McKinley, *Phys. Rev. Lett.* **123**, 248003 (2019).
- [32] A. Yamamoto, T. Inui, D. Suzuki, and K. Urayama, *Soft Matter* **19**, 9082 (2023).
- [33] K. Pham, G. Petekidis, D. Vlassopoulos, S. Egelhaaf, W. Poon, and P. Pusey, *J. Rheol.* **52**, 649 (2008).
- [34] K. A. Whitaker and E. M. Furst, *J. Rheol.* **60**, 517 (2016).
- [35] M. Pournajar, M. Zaiser, and P. Moretti, *Sci. Rep.* **12**, 11814 (2022).
- [36] M. Nabizadeh, F. Nasirian, X. Li, Y. Saraswat, R. Waheibi, L. C. Hsiao, D. Bi, B. Ravandi, and S. Jamali, *arXiv:2301.13027*.
- [37] L. C. Hsiao, R. S. Newman, S. C. Glotzer, and M. J. Solomon, *Proc. Natl. Acad. Sci.* **109**, 16029 (2012).
- [38] E. Moghimi, A. R. Jacob, N. Koumakis, and G. Petekidis, *Soft Matter* **13**, 2371 (2017).
- [39] T. Gibaud, N. Dagès, P. Lidon, G. Jung, L. C. Ahouré, M. Sztucki, A. Poulesquen, N. Hengl, F. Pignon, and S. Manneville, *Phys. Rev. X* **10**, 011028 (2020).
- [40] M. Das and G. Petekidis, *J. Chem. Phys.* **157**, 234902 (2022).